Pergamon

Int. J. Heat Mass Transfer. Vol. 40, No. 2, pp. 347–363, 1997

0017–9310/97 $15.00+0.00

PII: S0017–9310(96)00098–1

Changes of longitudinal vortex roll structure in a mixed convective air flow through a horizontal plane channel: an experimental study

M. Y. CHANG, C. H. YU and T. F. LIN†

Department of Mechanical Engineering, National Chiao Tung University, Hsinchu, Taiwan, Republic of China

(*Received* 27 *October* 1995 *and in final form* 6 *March* 1996)

Abstract—Flow visualization and temperature measurement were conducted to investigate the buoyancy induced longitudinal vortex flow structure in a mixed convective air flow through a bottom heated horizontal plane channel for the Reynolds number ranging from 20 to 50 and Rayleigh number from 6000 to 30 000. The results suggested that at low buoyancy-to-inertia ratio a longitudinal roll pair with spanwise symmetry is first induced near the duct sides and more rolls are induced adjacent to the existing rolls as the flow moves downstream. Steady vortex flow prevails after the initial transient. At high buoyancy-to-inertia ratio the splitting and merging of the rolls take place frequently causing the flow to become unsteady and highly asymmetric at high Rayleigh numbers. Several types of the roll splitting processes were identified, namely, the splitting of one roll to three rolls and two rolls to four rolls, formation of two new rolls and two successive roll splittings of the above types. The reverse processes were noted during the roll merging. The data from the measured time histories of the air temperature indicated that the flow oscillation is position dependent with the oscillation amplitude being higher in the downstream core regions. Besides, the oscillation amplitude inside a roll is determined largely by the spanwise or axial position adjustment during the roll splitting and merging processes. Finally, the data for the onset of steady and unsteady vortex flows were empirically correlated. Copyright © 1996 Elsevier Science Ltd.

1. INTRODUCTION

The buoyancy induced vortex flow structures at a high Gr/Re^2 in a mixed convective flow through a bottom heated horizontal flat duct play an important role in a number of technological processes such as cooling of microelectronic equipments, enhancing thermal efficiency of compact heat exchangers, collecting solar energy and others. The vortex flow in a horizontal duct normally appears in the form of longitudinal or transverse rolls depending on the Reynolds number. At a higher Gr/Re^2 these vortex rolls can be unsteady in time and can become wavy in space. In addition, during the time and space development the existing rolls may merge together and may split, and new rolls may be generated. The detailed understanding of these complicate temporal–spatial structural changes is relatively important in improving the thermal design of various engineering systems and is especially important in the growing of high purity single crystal from vapour phase. These changes in the vortex flow structures are more drastic in a duct of a higher aspect ratio since it provides more space for the rolls to move in the spanwise direction. In a series of studies [1–3], we have explored this complex vortex flow in a low aspect ratio rectangular duct ($A = 2$ and 4). An extension is made here to experimentally investigate the detailed vortex flow in a high aspect ratio duct with $A = 12$.

Detailed review of the literatures on the mixed convection in a bottom heated horizontal duct was conducted in our early study [1]. In the following only the most relevant works on this study are reviewed. The onset of the secondary flow due to thermal instability in mixed convection through a horizontal plane channel was experimentally found to be at the Rayleigh number around 1708 by Akiyama *et al.* [4] and Kamotani *et al.* [5]. This is also supported by the linear stability analysis [6–8]. Beyond this critical Rayleigh number, steady longitudinal rolls prevails and the spanwise temperature distribution has very regular sinusoidal shape and the roll number is equal to the aspect ratio [4]. The regular sinusoidal temperature distributions are distorted for $Re = 38$ as $Ra > 8000$ [9, 10]. A flow regime map in terms of Re vs Ra was proposed for nitrogen gas by Chiu and Rosenberger [11] and Chiu *et al.* [12] to locate the boundaries among the flow with no roll, steady and unsteady rolls. The flow structure in the thermal boundary layer

† Author to whom correspondence should be addressed.

NOMENCLATURE

A	aspect ratio, b/d
b	channel width
d	channel height
D	developing roll
FD	fully developed roll
g	gravitational acceleration
Gr	Grashof number $g\beta d^3(T_h-T_c)/\nu^2$
lb	left boundary
Ra	Rayleigh number $g\beta d^3(T_h-T_c)/\nu\alpha$
Re	Reynolds number $w_m d/\nu$
rb	right boundary
rc	roll center
T	temperature
T_m	mean temperature, $(T_h+T_c)/2$
t	dimensional time
w	axial velocity
x, y, z	dimensional Cartesian coordinates
X, Y, Z	dimensionless Cartesian coordinates, $x/d, y/d, z/d$.

Greek symbols

α	thermal diffusivity
β	thermal expansion coefficient
θ	dimensionless temperature $(T-T_m)/\Delta T$
ΔT	temperature difference between two plates, T_h-T_c
ν	kinematic viscosity
τ	dimensionless time, $t/(d/w_m)$.

Subscripts

c	cool surface
h	hot surface
m	average value.

was found to be influenced not only by Ra but also by the Froude number (Re^2/Gr) [10]. At very low Re the vortex is in the form of transverse rolls [13, 14].

A close examination of the above studies reveals that the important flow characteristics in the unsteady vortex flow in a bottom heated horizontal plane channel such as the development of the vortex rolls in the axial direction, the temporal structure of individual vortex roll and the mechanisms that destroy the orderly symmetric vortex structures are still not well understood. To complement these early studies, an experiment including detailed flow visualization and temperature measurement for a mixed convection of air in a horizontal plane channel is attempted here to explore the buoyancy induced unsteady longitudinal vortex flow structures ($20 \leqslant Re \leqslant 50$ and Ra up to 30000).

2. EXPERIMENTAL APPARATUS AND PROCEDURES

2.1. *Experimental apparatus*

A sketch of the established test apparatus for the mixed convection of air in a bottom heated horizontal plane channel and the adopted coordinate system are shown in Fig. 1. The test section is a rectangular duct of 240 mm wide and 300 mm long with the gap width of 20 mm between the hot and cold walls. Thus the aspect ratio of the duct is 12. The lower plate of the test section is made of a 15 mm thick, high purity copper plate and is electrically heated by d.c. power supplies. The heaters glued onto the outside surface of the bottom wall were divided into 10 segments in the flow direction and each heater was independently controlled by a GW GPC 3030D laboratory power supply. The width of the lower plate is 40 mm larger than that of the test section in order to reduce the edge effect of the test section. The upper plate of the test section is made of 3 mm thick glass plate. The plate is reinforced by a copper alloy frame to keep it flat. The upper plate is cooled by distilled water flowing above it. The distilled water is maintained at a constant temperature by a constant temperature circulator which consists of a heater, a cooler and a 90000 gallon underground water reservoir. This circulator can control the temperature of the distilled water within ± 0.1°C. The volume flow rate of the distilled cooling water is adjusted carefully so that the temperature difference in the cooling water over the glass plate is within ± 0.1°C. The water head is also suitably adjusted to minimize any possible deformation in the glass. The side walls of the test section are made of 5 mm thick plexiglass.

The temperature of the lower plate is measured by 13 calibrated and electrically insulated T-type thermocouples embedded in the plate. The temperature of the upper plate is measured by six T-type thermocouples stuck to the inside surface of the plate. The temperatures of both plates could be maintained at nearly uniform and constant values with the deviations ranging from ± 0.05°C to ± 0.12°C. For each experiment the top plate temperature is kept at the same values as that of the inlet air flow for the purpose of eliminating the formation of a thermal boundary layer on the top wall.

The open loop mixed convection apparatus begin with the air regulated from a 600 psi and 50000 cubic feet high pressure air tank which is passed through a settling chamber, a contraction nozzle and a developing channel before entering into the test section. In the settling chamber turbulence is suppressed by passing the air first through two fine mesh screens, then a honeycomb section and finally four fine mesh screens. The nozzle with a contraction ratio of 20 : 1 has been

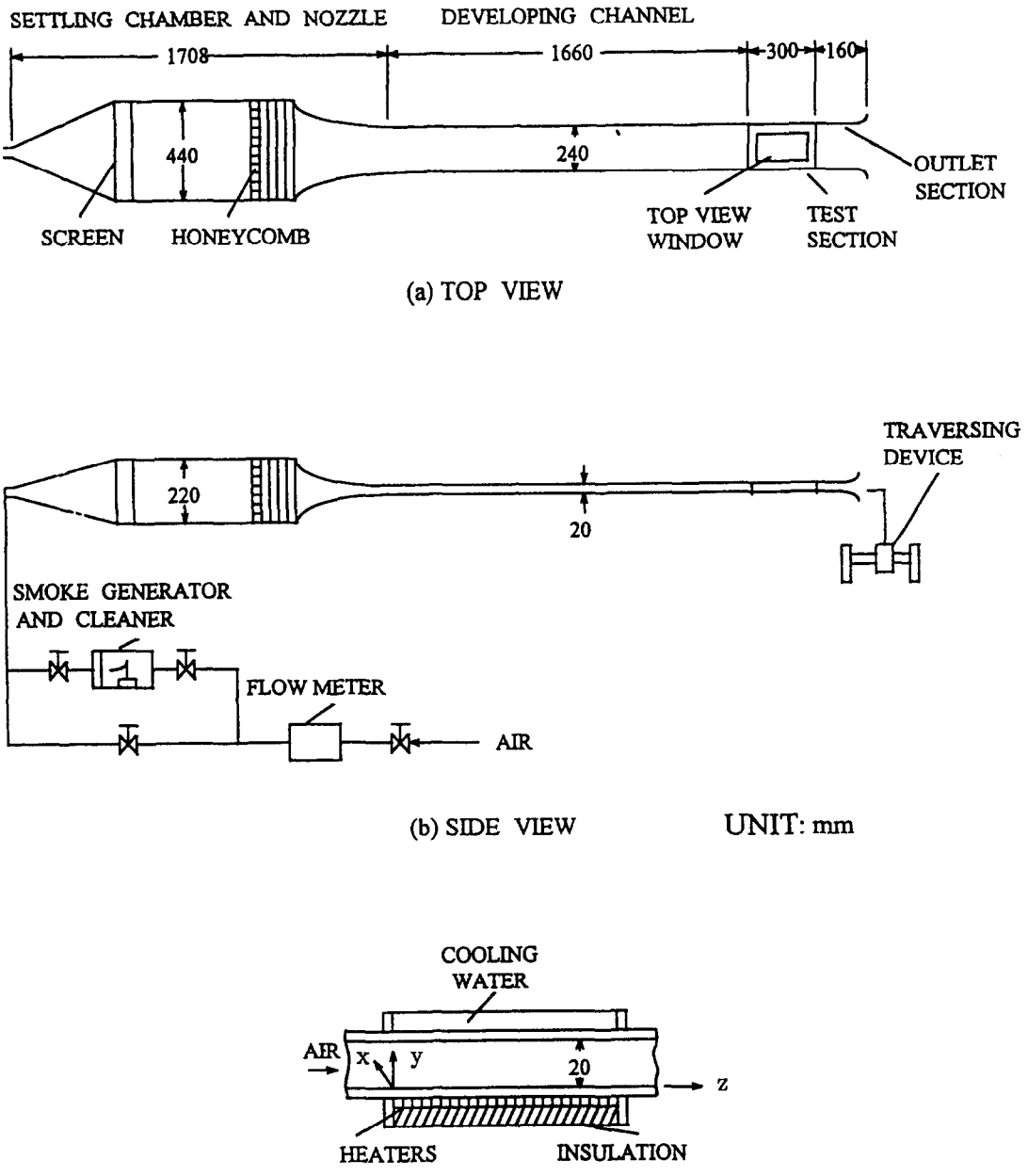

Fig. 1. Schematic of test apparatus and the chosen coordinate system.

designed to eliminate flow separation, minimize turbulence and provide a nearly uniform velocity at the inlet of the developing section. The developing section is 1660 mm in length, approximately 83 times of the channel height. This insures the flow being fully developed at the inlet of the test section for $Re \leqslant 50$. After the test section, a 160 mm outlet section is added to reduce the disturbance resulting from discharging the flow to the ambient. The settling chamber and the contraction nozzle are made of stainless steel, whereas the developing channel and the outlet section are made of 5 mm thick plexiglass. The whole test apparatus is placed in a quiescent house to eliminate any possible disturbance from the ambient outside the house. The entire loop is insulated with the superlon insulator of 20 mm thick and is mounted on a rigid supporting frame.

The volume flow rate of air is controlled and measured by a Hasting HFC flow controller with accuracy better than 1%. The flow measuring system is calibrated periodically by a Brooks bell prover with accuracy of 0.2%. The operating condition of the flowmeter in actual measurement is adjusted to a condition similar to that of calibration stand. The mean air speed in the test section is calculated from the total flow rate.

To measure the velocity and temperature distributions in the flow, probes are inserted from the downstream end of the test section. The probes are supported by a three-way traversing device. Velocity is measured by a hot-wire probe. For calibrating the hot-wire, the pipe flow method where the probe is placed in the center of a fully developed laminar pipe flow is used. The total flow rate is measured and the pipe center velocity is calculated from the parabolic distribution. Temperature is measured by a thermocouple probe which is an OMEGA (model HYP-O) mini hypodermic extremely small T-type thermocouple (33 gauge) implanted in a 1 inch long stainless steel hypodermic needle.

2.2. *Data uncertainty*

The data acquisition and control system and various instruments including a PC 486-66, multiplexers (Computer Products RTP 743 series), a digital barometer (Setra Systems 361B), reference junctions (Celesco Transducer Products BRJ 14), laboratory power supplies (GW GPC 3030D), OMEGA type T thermocouples, a Hasting HFC flow controller and a data reduction software are calibrated and adjusted end to end on site by Instrument Calibration Section, Q.A. Center, Chung Shan Institute of Science and Technology (CSIST), Taiwan with the transfer standards that the calibration hierarchy can trace back to the standards of National Institute of Standard and Technology (NIST), U.S.A. Before performing the end to end calibration all the sensors and transducers used were transported to CSIST for calibration or adjustment with the inter-lab standards based on the test point that will be encountered in the present test to get best calibration curve fit data. The main purpose of this calibration is to reduce any possible bias between the true physical value and the readout of the sensors and transducers. The data reduction error is reduced further by using the best nonlinear least square calibration curve fits and by selecting a suitable gain code of the multiplexers. The system is well ground and the electric noise signals are suitably filtered out. Fixed physical or simulated signals are then applied in the data uncertainty test. Samples higher than 32 are measured at each test point during the data uncertainty test. Uncertainties in the Rayleigh number, Reynolds number and other independent parameters were calculated according to the standard procedures established by Kline and McClintock [15] and Abernethy and Thompson [16]. The uncertainties due to the control unsteadiness and temperature nonuniformity are also accounted for in data uncertainty evaluation. In addition, the uncertainties of the thermal-physical properties of the air were also included in analysis. The detailed uncertainty analysis indicated that the uncertainties of temperature, volume flow rate, dimension, Reynolds number and Rayleigh number measurements are estimated to be less than $\pm 0.15^{\circ}C$, $\pm 1\%$, ± 0.05 mm, $\pm 2\%$ and $\pm 5\%$, respectively.

2.3. *Analysis of temperature oscillation*

The measured time-averaged temperature of the air flow are obtained by averaging 1000–3000 sampled data points depending on the magnitude and frequency of the oscillation at the detection point. The sampling rate of the data channel is set at 0.1 second per scan which is sufficiently high for the low frequency oscillation in the low Reynolds number mixed convective flow considered here. In the tests the detection points are distributed at 120 equi-spaced spanwise positions in the horizontal plane at $Y = 1/2$ and $Z = 2.52, 4.21, 5.89, 7.57, 9.26, 10.94, 12.62$ and 14.30. To further unravel the unsteady characteristics of the vortex rolls, the temperature oscillations in the roll centers and boundaries for selected rolls are also obtained. Note that the roll centers are in fact the locations where the dimensionless time-averaged temperature θ equal to zero and the roll boundaries are the locations where the time-avenged θ is at maximum or minimum.

2.4. *Preliminary investigation of flow field*

At first, the main forced flow is investigated to check its fully developed condition at the entrance of the test section with no heat input to the bottom plate. The data from the hot wire measurement clearly indicate that at the test section inlet the velocity profile is fully developed and is in good agreement with the analytical results given by Shah and London [17]. Additionally, the turbulence intensity is found to be less than 0.7%.

Flow visualization was conducted to observe the secondary flow patterns from the top and end views by injecting smoke at some distance ahead of the settling chamber. They were carried out by using a 1.5–2.5 mm plane light beam to shine through the flow field containing tiny incense particles as the light scattering centers and a sharp contrast could be achieved between the duct walls and the smoke.

In all the experiments to be reported below, we first imposed a fully developed flow in the entire test section and then turned on the power supply to the bottom plate and in the mean time circulated chilled water over the top plate. It took about 3 h for the Rayleigh number to rise to the test point and required about another 2 h for Ra to stabilize. After this we began various measurements and flow visualization.

3. EXPERIMENTAL RESULTS AND DISCUSSION

In the following only a small sample of the results is presented to manifest the effects of the Reynolds and Rayleigh numbers on the characteristics of the vortex flow.

3.1. *Spatial structure of vortex flow*

To illustrate the onset of the longitudinal vortex rolls at a low buoyancy-to-inertia ratio (Gr/Re^2), the flow photos taken from the top and end views at steady state for the case with $Re = 50$ and $Ra = 7000$ are shown in Fig. 2 respectively at the middle hori-

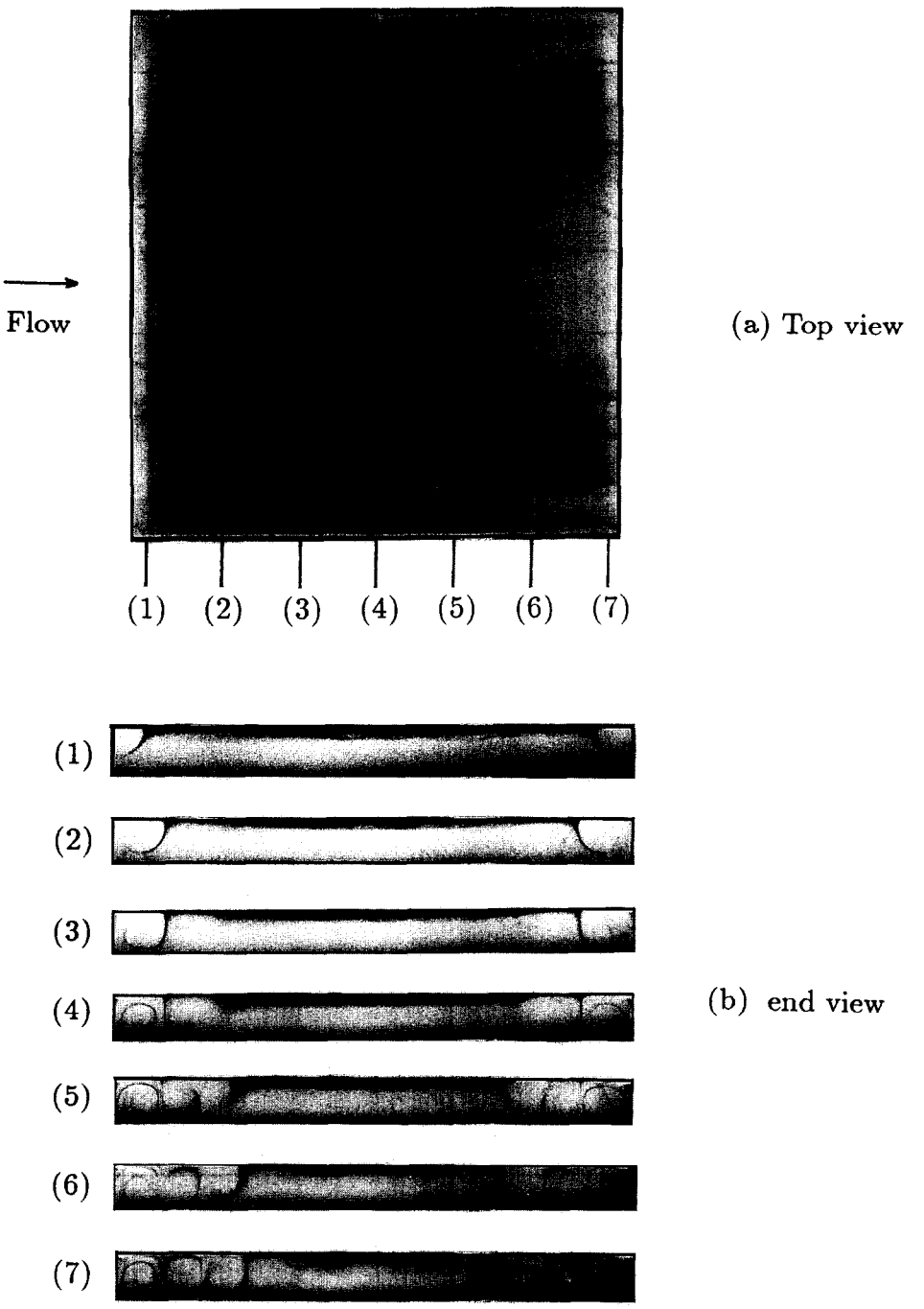

Fig. 2. Top view and cross-sectional view of the steady vortex, respectively at the midheight and at selected cross-sections for $Z = (1)\ 2.52$, (2) 4.21, (3) 5.89, (4) 7.57, (5) 9.26, (6) 10.94 and (7) 12.62 for $Re = 50$ and $Ra = 7000$.

zontal plane $Y = 1/2$ and at selected cross-sections. The results clearly indicate that immediately after the flow enters the test section two longitudinal rolls first appear in the regions near the side walls. Elsewhere, the flow is still unidirectional and hence is forced convection dominated. As the flow moves downstream, the existing rolls grow and meanwhile more rolls are induced. At $Z = 12.62$, three pairs of fully developed longitudinal rolls prevail near the side walls and additional rolls are about to be initiated in the core region of the duct, as suggested by the end view. It is noted from the present data that steady vortex flow prevails for $Ra < 8000$ when $Re = 50$. The longitudinal rolls are always initiated first from the side wall regions in the upstream and increase their number in pairs as the flow proceeds downstream. The maximum roll number is equal to or less than the aspect ratio of the duct. Thus the roll dimension is

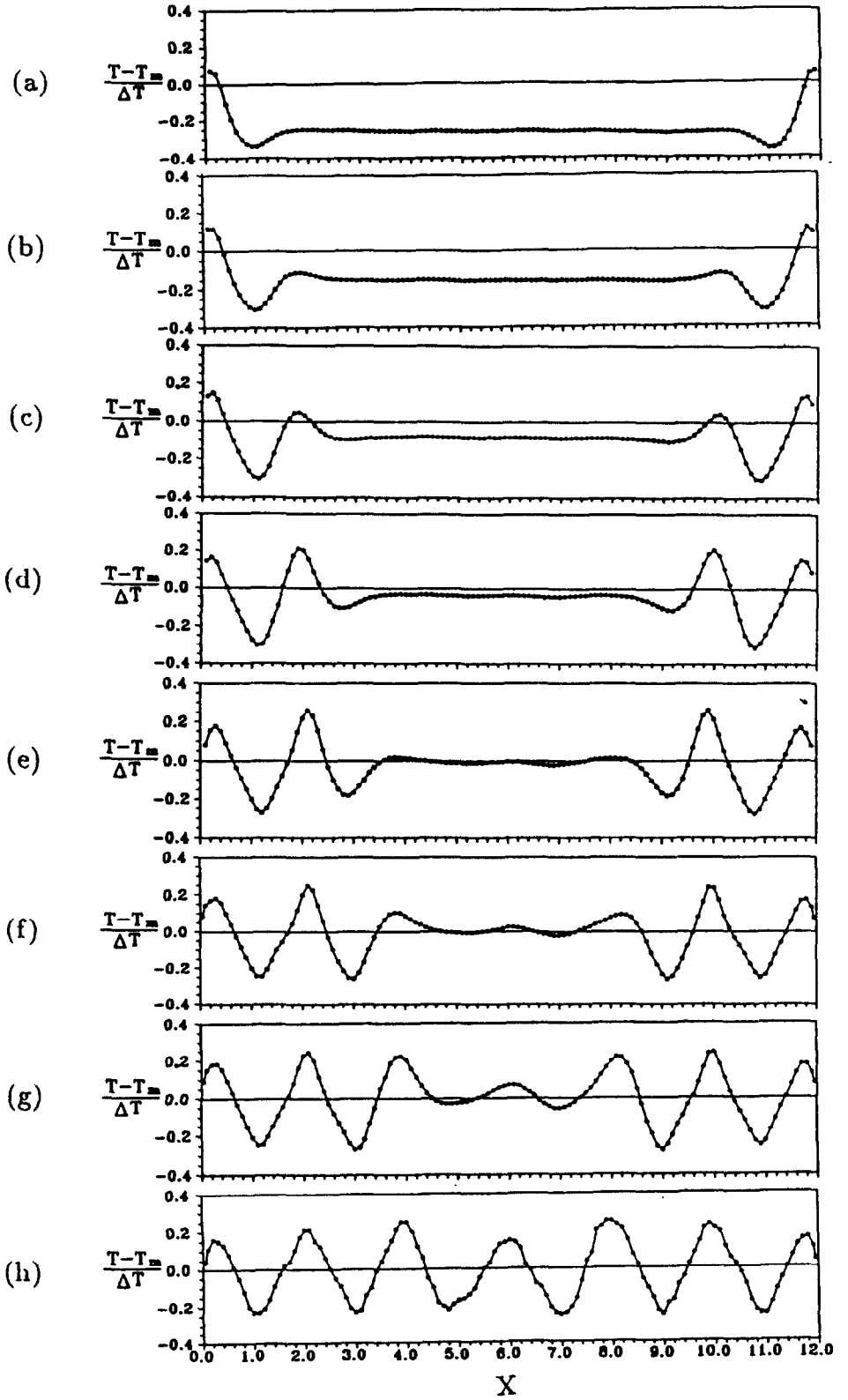

Fig. 3. Spanwise temperature distributions at the midheight at selected cross-sections Z = (a) 2.52, (b) 4.21, (c) 5.89, (d) 7.57, (e) 9.26, (f) 10.94, (g) 12.62 and (h) 14.30 for $Re = 50$ and $Ra = 7000$ in steady flow.

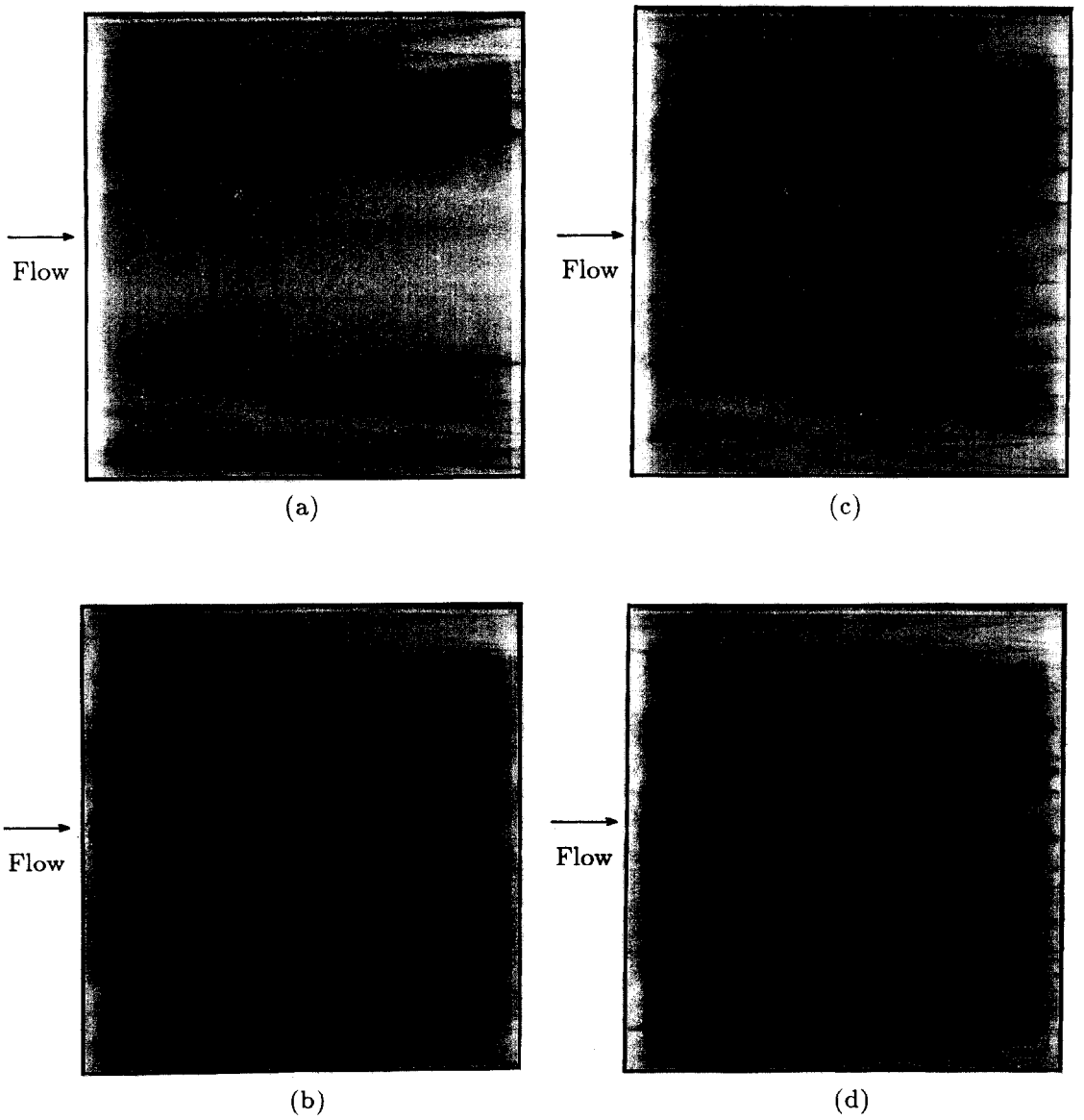

Fig. 4. Top view of the instantaneous vortex flow patterns at steady or statistical state for $Ra = 6000$ and (a) $Re = 50$, (b) $Re = 40$, (c) $Re = 30$ and (d) $Re = 20$.

nearly the same as the duct height. The rolls possess spanwise symmetry and grow regularly to a fully developed state as they proceed downstream. This unique roll structure results in the special spanwise temperature distributions at selected cross-sections shown in Fig. 3. The nearly regular sinusoidal spanwise temperature distributions near the side walls are in accordance with the existence of steady longitudinal rolls. Note that the temperature is above T_m in the region where the vortex flow is ascending, below T_m where it is descending and crosses the abscissa ($T = T_m$) near the roll center.

Next, the results for a higher Gr/Re^2 by decreasing the Reynolds number from 50 to 20 and fixing the Rayleigh number at 6000 are examined. Figures 4(a)–(d) show the top view of the flow at steady or statistical state long after the initial transients for $Ra = 6000$ and $Re = 50$, 40, 30 and 20. The results clearly manifest that at increasing Gr/Re^2 the onset of the vortex rolls moves upstream. Besides, for $Re \leqslant 40$ the flow is found to be unsteady. This flow unsteadiness is characterized by the cyclic vortex roll splitting in a certain period of time and combination in another period of time, as illustrated in Figs. 5(a) and (b) in which the vortices at the cross-section $Z = 12.62$ at selected time instants are displayed. It is noted from Fig. 5(a) that at $\tau = \tau_1$ twelve rolls (six pairs) with spanwise symmetry occupy the cross section. Later at $\tau = \tau_2$ one of these rolls, specifically the fourth roll numbering from the left side wall, grows to a larger size and meanwhile it squeezes the fifth roll. Then the larger roll splits into three small rolls at $\tau = \tau_3$. As time proceeds the small rolls gradually grow and the other rolls shrink slightly with the accompanying pos-

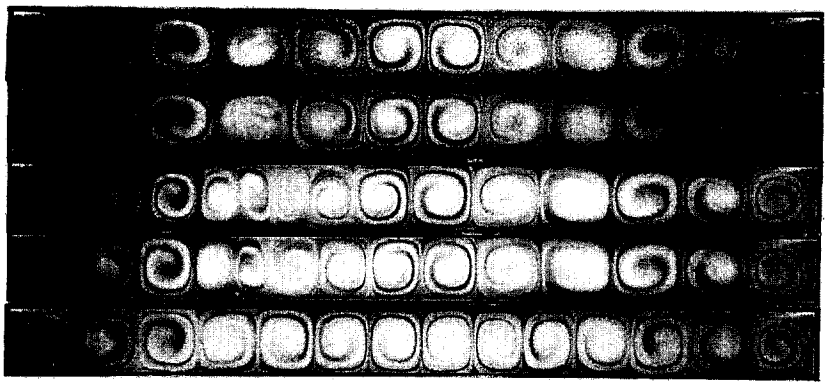

(a)

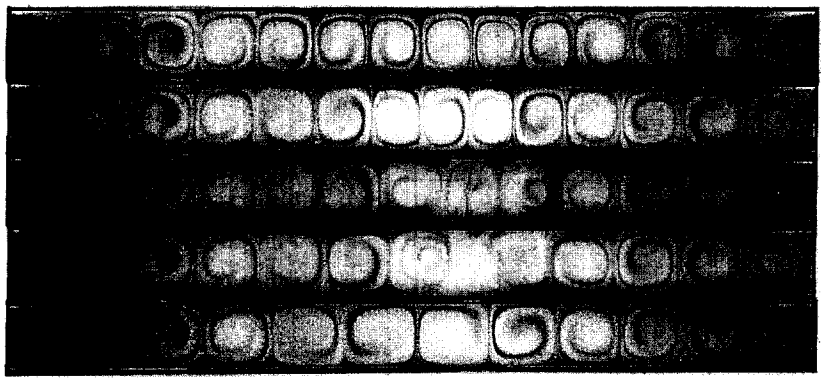

(b)

Fig. 5. Cross-sectional view of the vortex rolls at selected time instants at cross-section $Z = 12.62$ showing (a) the roll splitting and (b) roll merging for $Re = 20$ and $Ra = 6000$.

ition adjustment in the spanwise direction. At $\tau = \tau_5$ there are 14 symmetric and rather regular rolls (seven pairs) in the duct and the new roll generation process is completed. The reduction of the vortex pairs from seven to six pairs through the roll combination process shown in Fig. 5(b) begins with the simultaneous growth of certain rolls and shrink of several other rolls away from the duct sides, as evident from the pattern at $\tau = \tau_7$. Note that the three rolls near the vertical central plane at $X = A/2$ are smaller than the others. This process keeps going until the central roll in these three rolls becomes relatively weak and nearly disappears, as clearly seen at $\tau = \tau_9$. Then the other two rolls with the same direction of rotation start to gradually merge together. Beyond that the unevenly distributed rolls slowly adjust their sizes and positions. At $\tau = \tau_{10}$ the duct is occupied by six pairs of symmetric and regular rolls. It is worth while to mention that the above vortex flow possesses spanwise symmetry except in the processes of roll splitting and combination. Moreover, the above processes of roll splitting and merging do not occur periodically in time.

The vortex flow patterns associated with the increasing buoyancy-to-inertia ratio resulting from *Ra* raised from 8000 to 30 000 and *Re* fixed at 50 are examined by showing the instantaneous photographs from the top view for several typical cases given in Figs. 6(a)–(d). Again at a higher *Ra* the onset of vortex flow is initiated earlier and at a shorter distance from the duct inlet and the flow becomes time dependent for $Ra = 12\,000$, 20 000 and 30 000, similar to those discussed above for decreasing *Re*. However, several important differences do exist. A close inspection of the results for $Ra > 8000$ reveals that the vor-

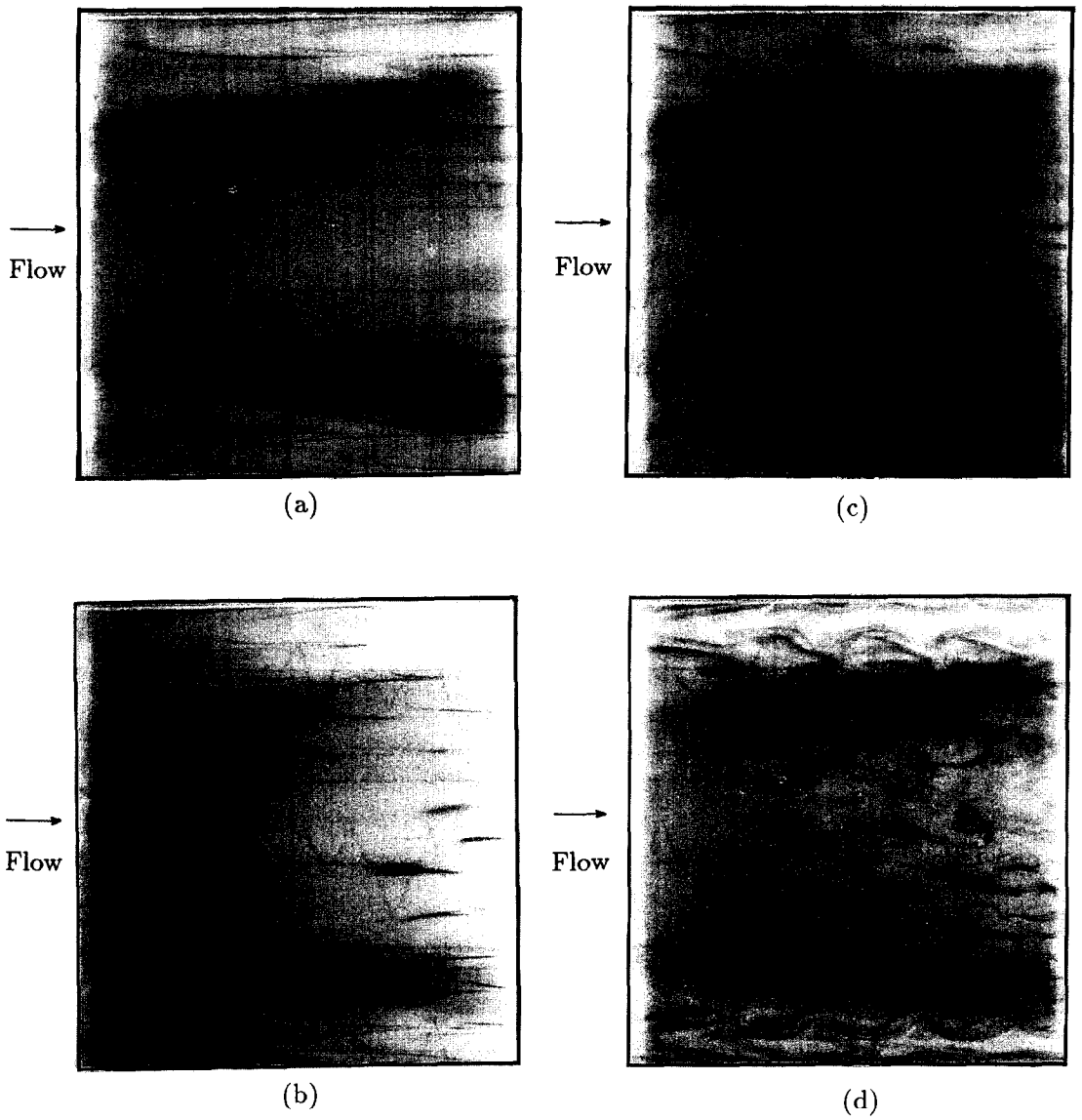

Fig. 6. Top view of the instantaneous vortex flow patterns at steady or statistical state for $Re = 50$ and (a) $Ra = 8000$, (b) $Ra = 12000$, (c) $Ra = 20000$ and (d) $Ra = 30000$.

tex rolls are asymmetric at most times in the region slightly beyond the onset point. This is supported by examining the time-averaged spanwise temperature distributions at the middle horizontal plane at selected cross sections displayed in Fig. 7 for $Re = 50$ and $Ra = 20000$. Note that the time-averaged air temperature is no longer in spanwise symmetry for $Z \geqslant 5.0$. Moreover, we observed more frequent roll splitting and merging at this higher Ra. In particular, there are six to eight pairs of vortex rolls existing in the duct. Near the onset point the rolls are usually small and eight pairs are prevalent, but six pairs dominate near the exit end where the rolls are larger due to the roll growth in the axial direction. This again can be inferred from the spanwise temperature distributions in Fig. 7. It is of interest to point out that the unstable roll splitting and merging cause the newly formed rolls and their neighboring rolls to unsteadily move back and forth in the axial direction. This in turn results in the tilting of the roll patterns at the onset point, as exemplified in Figs. 8(a)–(d) for $Re = 50$ and $Ra = 30000$. Additionally, in Figs. 8(c) and (d) the roll merging in the exit region and in both the upstream and downstream regions is also illustrated.

The formation of new vortex rolls at high Gr/Re^2 deserves more discussion. In addition to the new roll generation through the splitting of one roll into three rolls already shown in Fig. 5, we also observed the breaking of two rolls into four rolls and the generation

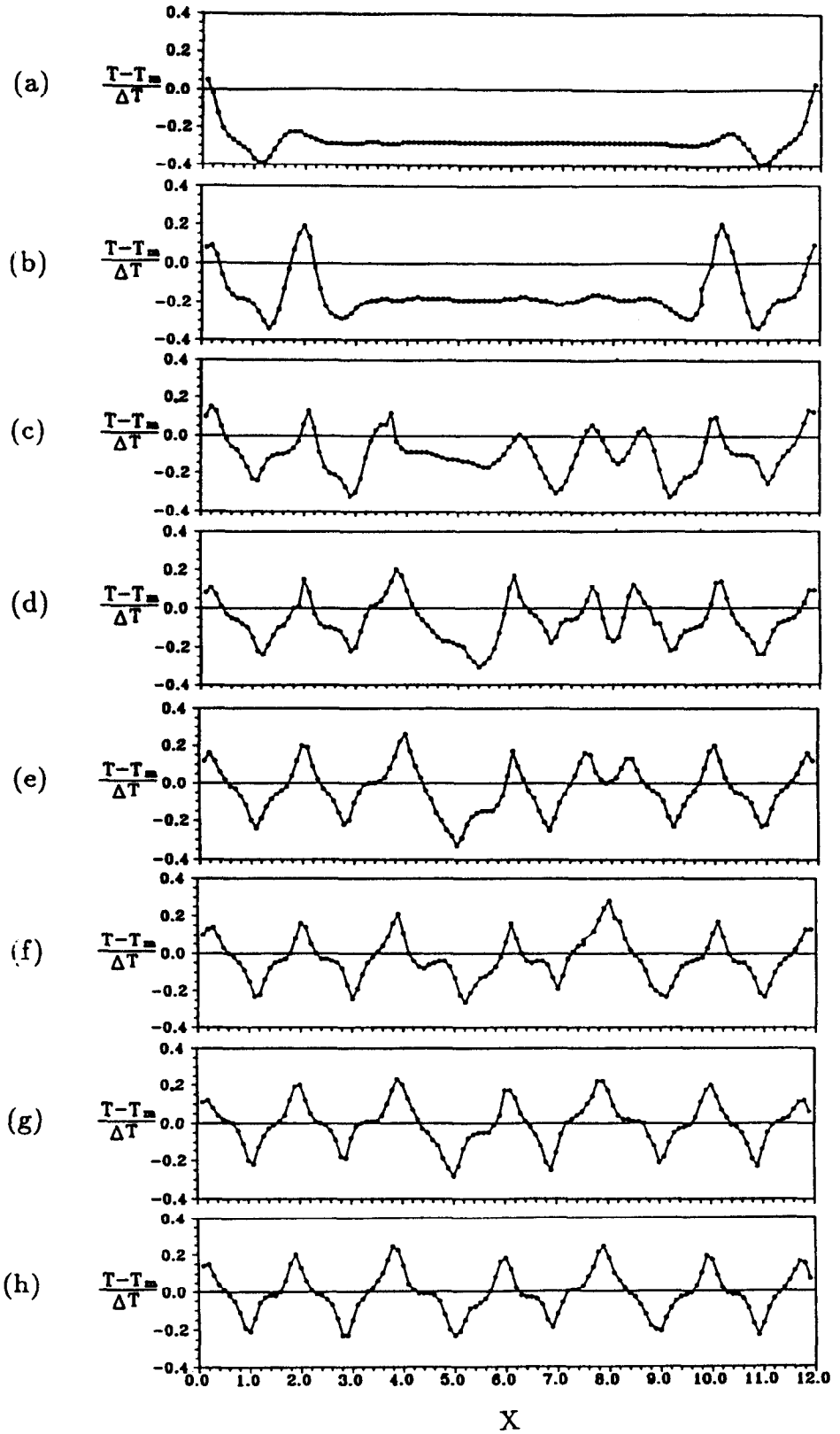

Fig. 7. Time-averaged spanwise temperature distributions at the midheight at selected cross-sections Z = (a) 2.52, (b) 4.21, (c) 5.89, (d) 7.57, (e) 9.26, (f) 10.94, (g) 12.62 and (h) 14.30 for $Re = 50$ and $Ra = 20\,000$.

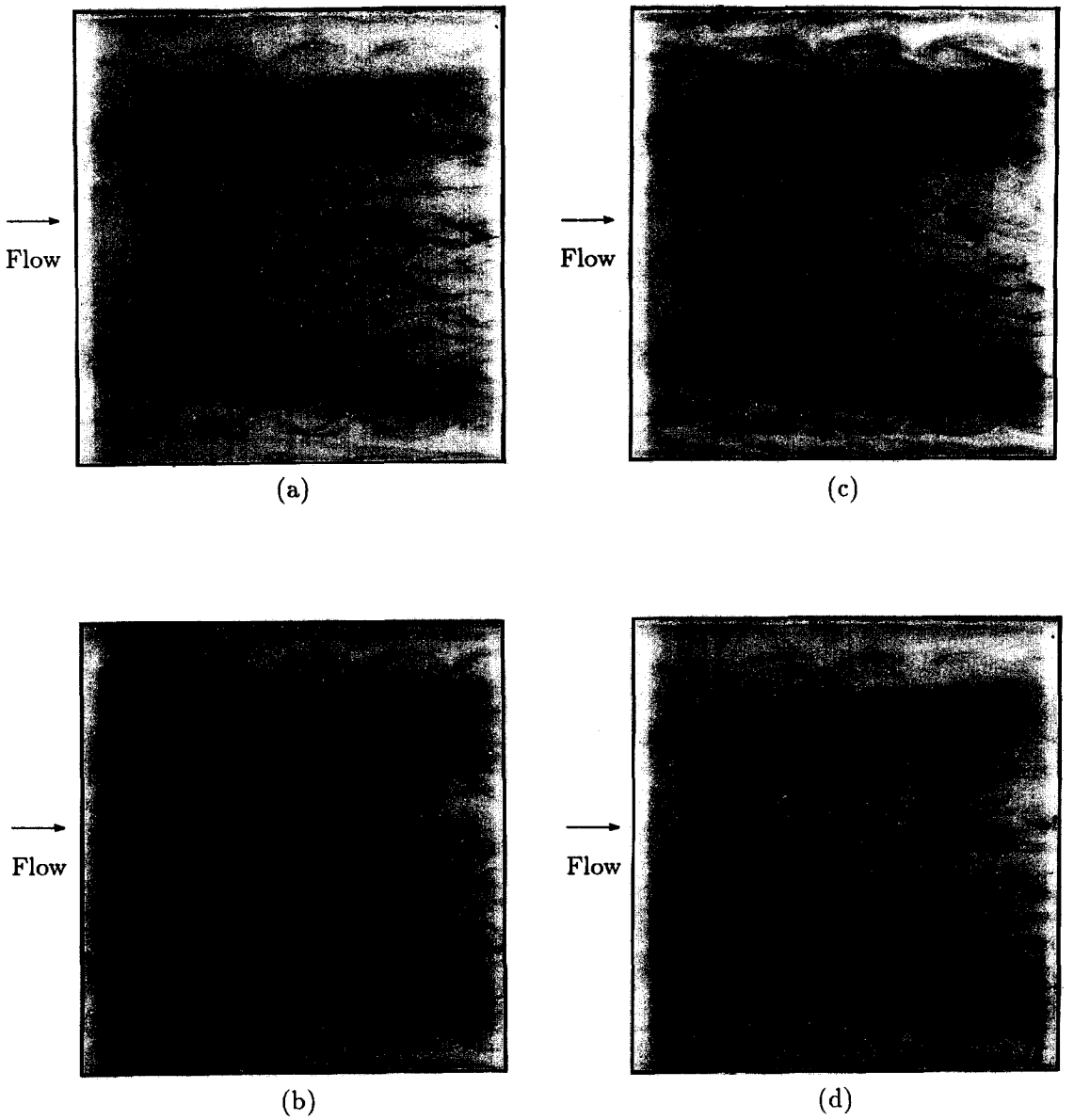

Fig. 8. Instantaneous vortex flow patterns for $Re = 50$ and $Ra = 30\,000$ showing (a) symmetric onset of vortex roll, (b) tilt of onset point, (c) merging of rolls in downstream core region and (d) merging of rolls in both upstream and downstream core regions.

of brand new rolls driven by the thermals from the heated bottom plate. These are respectively exemplified in Figs. 9(a) and (b) for $Re = 30$ and $Ra = 9000$. The former mode of the roll generation usually prevails in the downstream region for a high Ra flow, while the latter mode normally appear near the onset point where the rolls are smaller and more room is available for the new rolls to be generated. Finally, it is of interest to point out that in the downstream region the increase of the roll number from six to eight pairs is normally through the two consecutive roll splitting processes before any roll combination takes place. Thus, the roll pattern changes from six to seven pairs and then to eight pairs.

3.2. *Temporal structure of vortex flow*

Up to this point attention has been focused on the spatial structure of the longitudinal vortex flow. To illustrate temporal characteristics in the unsteady flow, the time records of the air temperature at the statistical state at a number of locations at the roll center and roll boundaries for selected rolls at selected cross sections are given in Fig. 10 for $Re = 20$ and $Ra = 6000$ and in Fig. 11 for $Re = 50$ and $Ra = 20\,000$. These records indicate that the temperature oscillation is position dependent. Besides, the oscillation is initiated from the downstream core region and decays significantly towards the side walls and upstream region. Comparing the time histories at

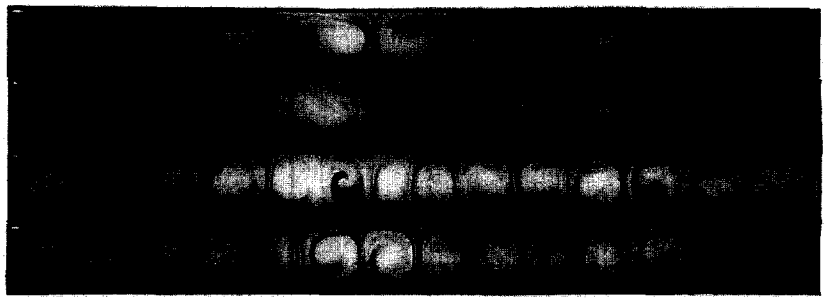

(a) Z=12.62

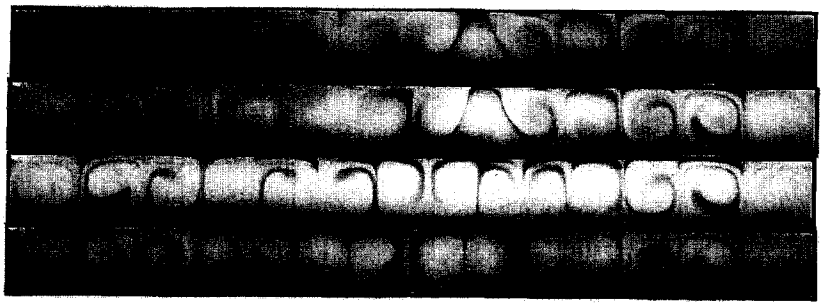

(b) Z=9.26

Fig. 9. Cross plane vortex flow patterns at selected time instants for $Re = 30$ and $Ra = 9000$ at two cross-sections showing the formation of new rolls: (a) splitting of two rolls into four rolls and (b) generation of two brand new rolls.

the corresponding points symmetric with respect to the vertical central plane $X = A/2$ discloses that the time oscillation patterns are similar at the corresponding points for the case with $Ra = 6000$ and $Re = 20$, but are somewhat different at $Ra = 20000$ and $Re = 50$. This obviously results from the asymmetric roll patterns for the high Rayleigh number flow discussed above. It is also noted that the amplitudes and phases of the oscillation at the roll center and boundaries for a given roll can differ substantially. Moreover, no time periodic oscillation was ever detected in the experiment. The oscillation amplitude is either rather small, implying the flow being steady, or discernible but is irregular. The nonexistence of the periodic flow is attributed to the large aspect ratio ($A = 12$) of the duct, which allows many vortex rolls to be generated and to interact in complex way. When the aspect ratio is reduced to six we did observe the time periodic flow.

Several types of the temperature oscillation can be identified in accordance with the spatial vortex flow patterns, as discussed in Section 3.1. Downstream of the onset point the vortex flow is usually steady and in the developing stage with the roll diameter growing gradually in the axial direction. The associated time records at the roll center and boundaries are like those shown in Fig. 12(a). Further downstream the vortex flow slowly evolves to a fully developed state in which the roll size does not change with z and the flow is also steady, as illustrated by the data in Fig. 12(b). The temperature oscillation in the unsteady flow associated with the small spanwise position adjustment during the splitting and merging of the rolls is presented in Fig. 12(c). At the roll center the oscillation is rather intense, but at the roll boundaries no temperature oscillation is detected. The axial oscillation of the vortex rolls during the roll splitting and merging at high Rayleigh numbers causes the roll boundaries to oscillate with time in a much larger amplitude than that at the roll center, as given in Fig. 12(d). Downstream of the above unsteady flow regions the vortex rolls become more irregular and oscillate everywhere in the rolls. This type of oscillation is shown in Fig. 12(e) for mild irregularity and in Fig. 12(f) for larger amplitude chaotic situation.

3.3. *Onset of steady and unsteady vortex flows*

Data for the onset of the steady and unsteady vortex flows deserve some discussion. For clarity a snapshot of the top view of the vortex flow for the case with

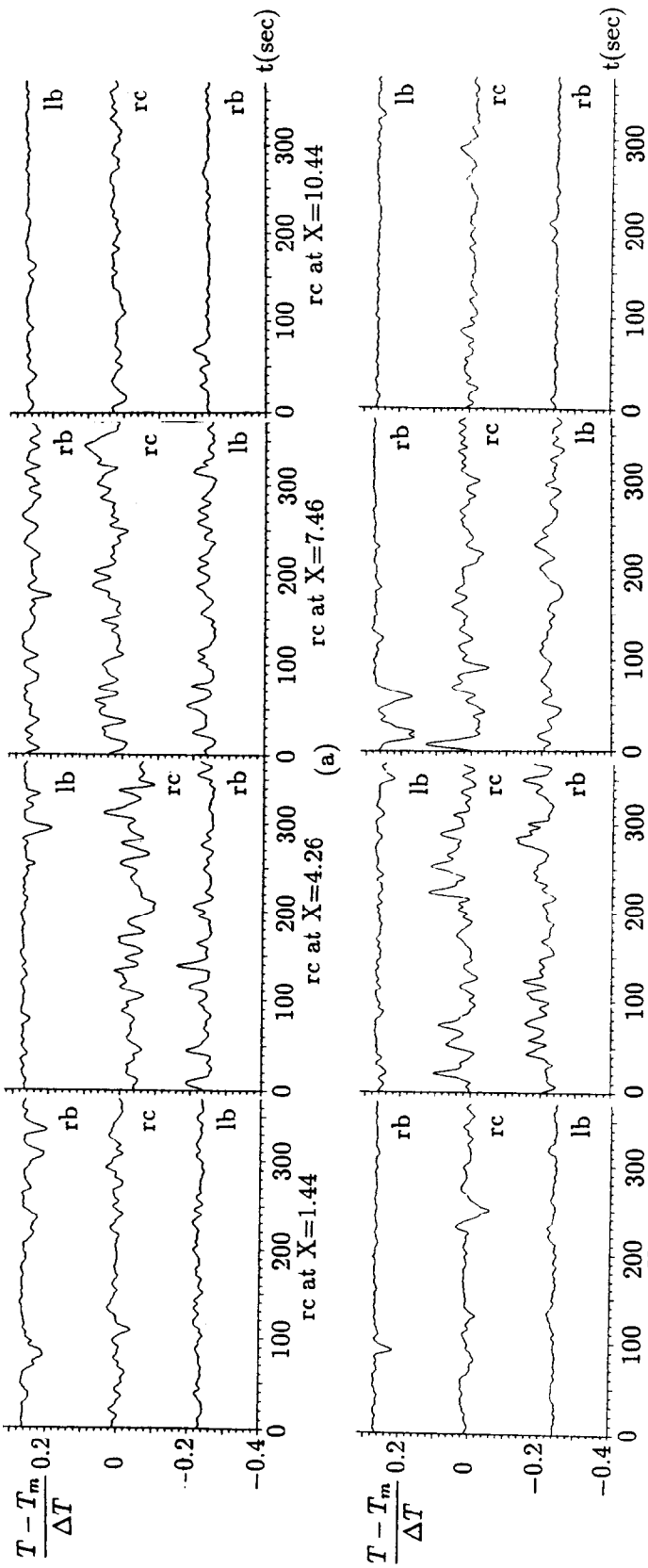

Fig. 10. Time records of the air temperature at selected roll centers (rc), left roll boundaries (lb) and right roll boundaries (rb) at the midheight for $Re = 20$ and $Ra = 6000$ at selected cross-sections $Z =$ (a) 14.30, (b) 12.62 and (c) 9.26

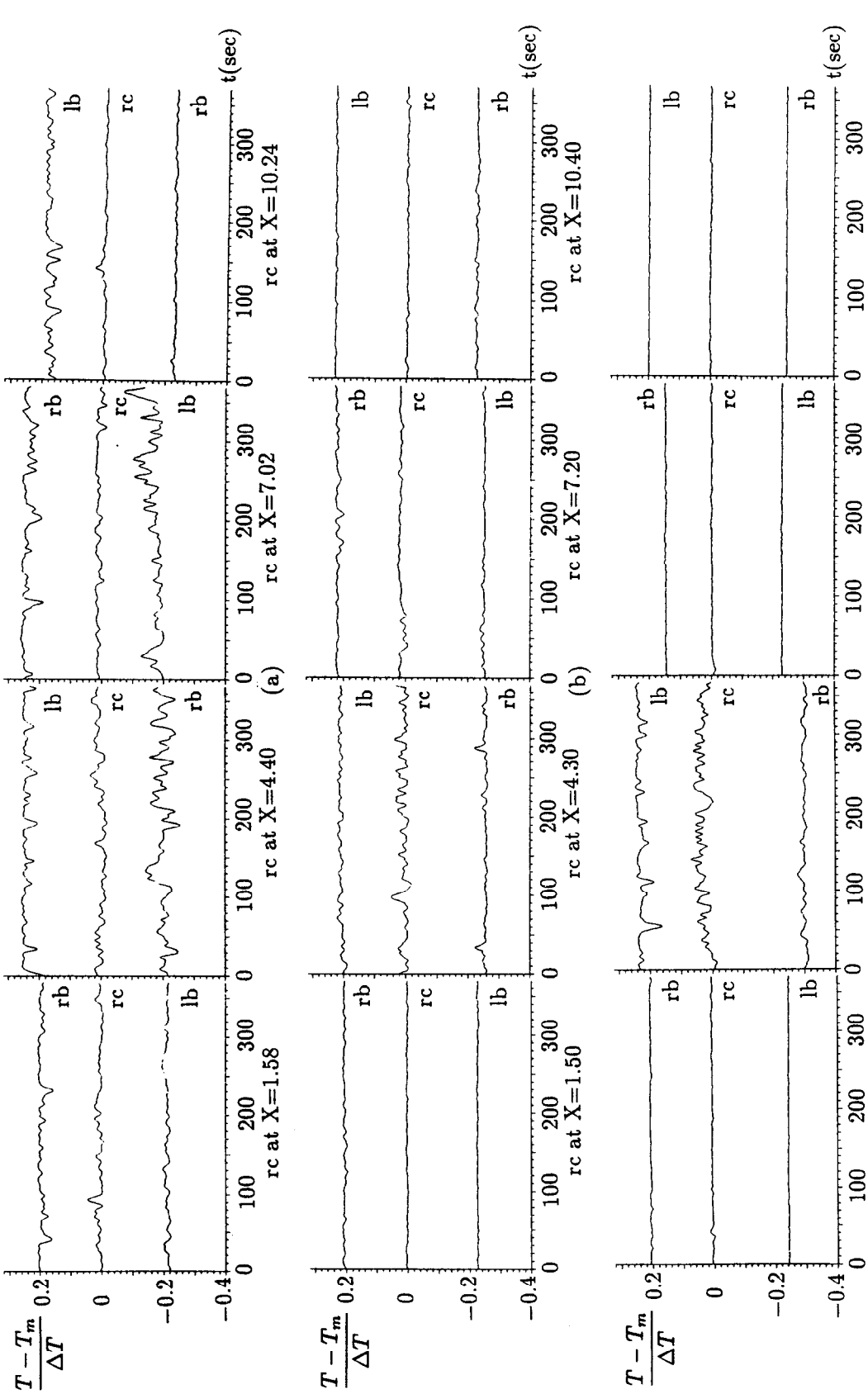

Fig. 11. Time histories of the air temperature at selected roll centers (rc), left roll boundaries (lb) and right roll boundaries (rb) at the midheight for $Re = 50$, and $Ra = 20\,000$ at selected cross-sections Z = (a) 14.30, (b) 12.62 and (c) 9.26.

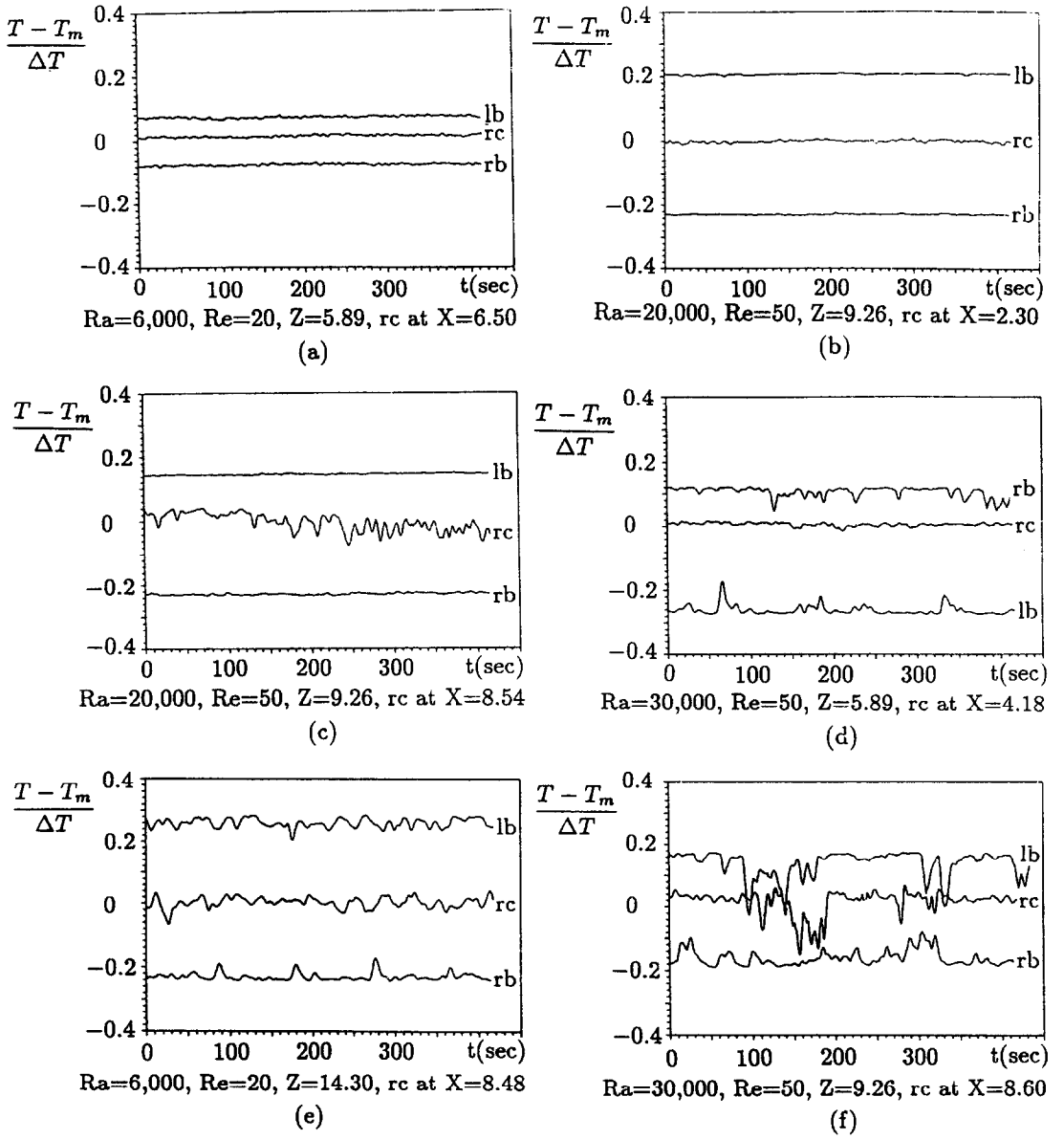

Fig. 12. Time records of the air temperature at selected roll centers (rc) and boundaries (lb and rb) showing the temporal oscillations in a (a) steady developing roll, (b) steady fully developed roll, (c) roll affected by spanwise position adjustment, (d) roll affected by the axial oscillation, (e) roll affected by new roll generation and (f) chaotic flow.

$Ra = 7000$ and $Re = 20$ is shown in Fig. 13 as an example. The results again indicate that in the entry region two longitudinal rolls first appear near the side walls. As the flow moves downstream , more rolls are induced. The above results also clearly suggest that the onset point depends on the spanwise location. If the onset point of the steady vortex flow in the entire duct is taken as the location at which the second pair of the roll is initiated, our experimental data can be correlated as

$$Z_1 = 75 \times \left(\frac{Re^{1.4}}{Ra}\right)^{0.7} \quad (1)$$

where Z is the dimensionless axial coordinate. The predicted onset point is close to other experimental measurements (Kamotani *et al.* [5] and Chiu and Rossenberger [11]) and stability analysis (Lee and Hwang [8]). If the onset point is chosen to be the location where the third roll pair is initiated, our data can be correlated as

$$Z_2 = 100 \times \left(\frac{Re^{1.4}}{Ra}\right)^{0.7}. \quad (2)$$

This predicted onset point locates close to our numerical prediction where a third-order upwind finite difference scheme was chosen to directly solve the three-dimensional (3D) Navier–Stokes and energy equations [18]. In this numerical simulation the onset

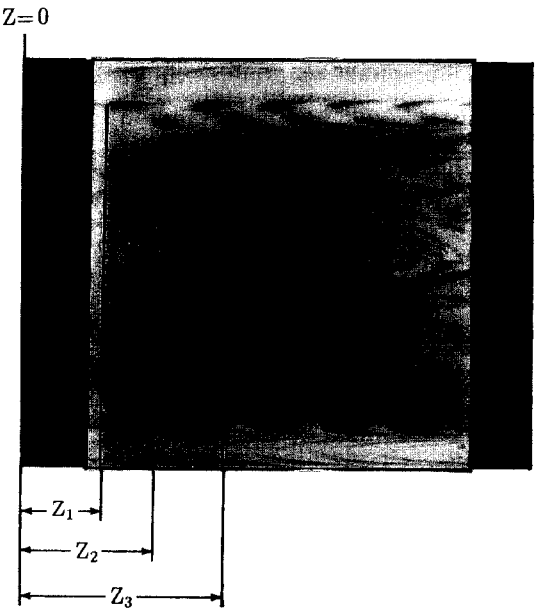

Fig. 13. Instantaneous vortex flow pattern viewing from the top illustrating the onset of steady and unsteady vortex rolls for $Ra = 7000$ and $Re = 20$.

Table 1. Comparison of experimentally and numerically predicted major flow characteristics

Case		Onset of vortex flow			Roll number (pairs)		Flow state
Ra	*Re*	Experiment	Computation [18]	Equation (2)	Experiment	Computation [18]	(steady or unsteady)
6000	50	10.2	11.2	10.5	4 FD+1 D	4 FD+2 D	steady
6000	40	8.2	—	8.4	6–8	—	unsteady
6000	30	6.2	—	6.4	6–7	—	unsteady
6000	20	4.3	—	4.3	6–7	—	unsteady
7000	50	9.2	10.5	9.4	5 FD+1 D	5 FD+1 D	steady
8000	50	8.8	9.4	8.6	6	5 FD+1 D	steady
9000	50	8.0	8.8	7.9	6–7	6	unsteady
9000	40	6.2	5.8	6.3	6–8	6–8	unsteady
9000	30	4.7	4.2	4.8	6–8	6–8	unsteady
9000	20	3.2	3.6	3.2	5–8	5–8	unsteady
10000	50	7.7	7.1	7.3	6–7	6–8	unsteady
12000	50	6.6	5.2	6.5	6–8	7–8	unsteady
12000	40	4.9	4.1	5.2	6–8	6–7	unsteady
12000	30	3.6	3.6	3.9	6–8	6–7	unsteady
15000	50	5.4	5.2	5.5	6–8	6–7	unsteady
20000	50	5.2	3.6	4.5	6–8	6–7	unsteady
30000	50	3.8	3.3	3.4	6–8	6–7	unsteady

point is defined as the location at which the spanwise average Nusselt number enhanced by the vortex flow exceeds the forced convection by 3%. The computational data are given in Table 1 and compared with our measured data. Comparison of the roll number and flow conditions for some sampled cases is also shown in the table. Qualitative agreement is noted.

The flow visualization discussed above has shown that the roll splitting and merging is the main cause leading to the breakdown of the steady state. Thus, it is appropriate to define the onset of unsteady vortex as the location at which the maximum number of the rolls is initiated. Our experimental results for the onset of the unsteady vortex flow can be correlated as

$$Z_3 = 138 \times \left(\frac{Re^{1.4}}{Ra}\right)^{0.7}. \quad (3)$$

4. CONCLUDING REMARKS

In the present study an experimental investigation through detailed flow visualization and temperature measurement has been carried out to explore the spatial and temporal structures of the buoyancy induced vortex flow in a mixed convection of air in a bottom heated horizontal plane channel for $Re \leqslant 50$. At a low buoyancy-to-inertia ratio the longitudinal vortex rolls are successively induced beginning from the regions

near the side walls as the flow moves downstream. The flow is spanwisely symmetric and reaches steady state after the initial transient. At a high buoyancy-to-inertia ratio with a decreasing Reynolds number or increasing Rayleigh number, the vortex flow becomes unsteady due to the presence of roll splitting and merging. A few different roll splitting and merging processes were identified and examined in detail. Rolls ranging from six to eight pairs were observed in the duct. The time oscillation of the flow inferred from the temperature measurement is position dependent and is significantly affected by the flow motion induced during the roll splitting and merging processes. In addition, correlations for the onset of steady and unsteady vortex flows were proposed.

During the course of this investigation it has been realized that the vortex flow is in the form of moving transverse rolls when Re is below 15. The characteristics of the transverse rolls and the transformation from the longitudinal to transverse roll structures or the reverse process require further study.

Acknowledgement—The financial support of this study by the engineering division of National Science Council of Taiwan, R.O.C. through the contract NSC83-0404-E-009-054 is greatly appreciated.

REFERENCES

1. C. C. Hwang and T. F. Lin, Buoyancy induced flow transition in mixed convective flow of air through a bottom heated horizontal rectangular duct, *Int. J. Heat Mass Transfer* **37,** 1235–1255 (1994).
2. C. C. Hwang and T. F. Lin, Vortex flow and thermal characteristics in mixed convection of air in a horizontal rectangular duct; effects of the Reynolds and Grashof numbers, *Int. J. Heat Mass Transfer* **38,** 1661–1674 (1995).
3. W. L. Lin and T.-F. Lin, Experimental study of unstable mixed convection of air in a bottom heated horizontal rectangular duct, *Int. J. Heat Mass Transfer* **39,** 1649–1663 (1996).
4. M. Akiyama, G. J. Hwang and K. C. Cheng, Experiments on the onset of longitudinal vortices in laminar forced convection between horizontal planes, *J. Heat Transfer* **93,** 335–341 (1971).
5. Y. Kamotani, S. Ostrach and H. Miao, Convection heat transfer augmentation in thermal entrance regions by means of thermal instability, *J. Heat Transfer* **101,** 222–226 (1979).
6. W. Nakayama, G. J. Hwang and K. C. Cheng, Thermal instability in plane poiseuille flow, *J. Heat Transfer* **92,** 61–68 (1970).
7. G. J. Hwang and K. C. Cheng, Convective instability in the thermal entrance region of a horizontal parallel-plate channel heated from below, *J. Heat Transfer* **95,** 72–77 (1973).
8. F. S. Lee and G. J. Hwang, Transient analysis on the onset of thermal instability in the thermal entrance region of a horizontal parallel plate channel, *J. Heat Transfer* **113,** 363–370 (1991).
9. S. Ostrach and Y. Kamotani, Heat transfer augmentation in laminar fully developed channel flow by means of heating from below, *J. Heat Transfer* **97,** 220–225 (1975).
10. Y. Kamotani and S. Ostrach, Effect of thermal instability on thermally developing laminar channel flow, *J. Heat Transfer* **98,** 62–66 (1976).
11. K. C. Chiu and F. Rosenberger, Mixed convection between horizontal plates—I. Entrance effects, *Int. J. Heat Mass Transfer* **30,** 1645–1654 (1987).
12. K. C. Chiu, J. Ouazzani and F. Rosenberger, Mixed convection between horizontal plates—II. Fully developed flow, *Int. J. Heat Mass Transfer* **30,** 1655-1662 (1987).
13. M. T. Ouazzani, J. P. Caltagirone, G. Meyer and A. Mojtabi, Etude numérique et expérimental de la convection mixte entre deux plans horizontaux a températures differents, *Int. J. Heat Mass Transfer* **32,** 261–269 (1989).
14. M. T. Ouazzani, J. K. Platten and A. Mojtabi, Etude expérimental de la convection mixte entre deux plans horizontaux à températures différents—II, *Int. J. Heat Mass Transfer* **33,** 1417–1427 (1990).
15. S. J. Kline and F. A. McClintock, Describing uncertainties in single-sample experiments, *Mech. Engng* **75,** 3–12 (1953).
16. R. B. Abernethy and J. W. Thompson, Jr., Handbook—Uncertainty in gas turbine measurements, Technical Report No. AEDC-TR-73-5(AD-755356) March (1973).
17. R. K. Shah and A. L. London, *Laminar Flow Forced Convection in Ducts*, pp. 196–198. Academic Press, New York (1987).
18. C. H. Yu, M. Y. Chang, C. C. Hwang and T.-F. Lin, Unsteady vortex roll structures in a mixed convective air flow through a horizontal plane channel: a numerical study, *Int. J. Heat Mass Transfer* (in press).